American Mineralogist, Volume 97, pages 1812–1815, 2012

LETTER

The crystal structure of bartelkeite, with a revised chemical formula, $PbFeGe^{VI}(Ge_2^{IV}O_7)(OH)_2 \cdot H_2O$, isotypic with high-pressure $P2_1/m$ lawsonite

MARCUS J. ORIGLIERI,[1] HEXIONG YANG,[1,*] ROBERT T. DOWNS,[1] ESTHER S. POSNER,[1] KENNETH J. DOMANIK,[2] AND WILLIAM W. PINCH[3]

[1]Department of Geosciences, University of Arizona, Tucson, Arizona 85721-0077 U.S.A.
[2]Lunar and Planetary Laboratory, University of Arizona, Tucson, Arizona 85721-0092 U.S.A.
[3]19 Stonebridge Lane, Pittsford, New York 14534, U.S.A.

ABSTRACT

Bartelkeite from Tsumeb, Namibia, was originally described by Keller et al. (1981) with the chemical formula $PbFeGe_3O_8$. By means of electron microprobe analysis, single-crystal X-ray diffraction, and Raman spectroscopy, we examined this mineral from the type locality. Our results show that bartelkeite is monoclinic with space group $P2_1/m$, unit-cell parameters $a = 5.8279(2)$, $b = 13.6150(4)$, $c = 6.3097(2)$ Å, $\beta = 127.314(2)°$, and a revised ideal chemical formula $PbFeGe^{VI}Ge_2^{IV}O_7(OH)_2 \cdot H_2O$ ($Z = 2$). Most remarkably, bartelkeite is isostructural with the high-pressure $P2_1/m$ phase of lawsonite, $CaAl_2Si_2O_7(OH) \cdot H_2O$, which is only stable above 8.6 GPa and a potential host for H_2O in subducting slabs. Its structure consists of single chains of edge-sharing FeO_6 and $Ge1O_6$ octahedra parallel to the *c*-axis, cross-linked by $Ge2_2O_7$ tetrahedral dimers. The average <Ge-O> bond lengths for the GeO_6 and GeO_4 polyhedra are 1.889 and 1.744 Å, respectively. The Pb atoms and H_2O groups occupy large cavities within the framework. The hydrogen bonding scheme in bartelkeite is similar to that in lawsonite. Bartelkeite represents the first known mineral containing both 4- and 6-coordinated Ge atoms and may serve as an excellent analog for further exploration of the temperature-pressure-composition space of lawsonite.

Keywords: Bartelkeite, germanate, hydrous mineral, crystal structure, X-ray diffraction, Raman spectra

INTRODUCTION

Germanate materials are used as analogues of silicate phases because they can be studied at attainable experimental conditions and provide an understanding of the physical and chemical properties of minerals and melts in the Earth's interior (e.g., Ringwood, and Seabrook 1963; Ross et al. 1986; Hazen et al. 1996; Henderson and Wang 2002; Iezzi et al. 2005; Nestola et al. 2008). Yet, little attention has been devoted to the Ge-analogues of *hydrous* silicates thus far (Thomas et al. 2008), despite their presumed role in the hydrogen budget of the earth (e.g., Ringwood and Major 1967; Thompson 1992; Frost 2006). Only a few high-pressure hydrous germanates in the Al_2O_3-GeO_2-H_2O system have been examined as analogs for phases in the Al_2O_3-SiO_2-H_2O system in deeply subducted rocks, where lawsonite and related phases undergo phase transformations (e.g., Schmidt 1995; Wunder and Marler 1997).

While it appears that the number of synthetic germanates has been increasing continuously, there are only 3 anhydrous and 10 hydrous natural germanates in the current list of IMA approved minerals. Unfortunately, until now, seven of these germanate minerals have not been structurally characterized, making it difficult to take full advantage of natural germanates as models of silicates at mantle conditions.

The germanate, bartelkeite, was originally described by Keller et al. (1981) as a new mineral from Tsumeb, Namibia, with chemical formula $PbFeGe_3O_8$, and monoclinic symmetry with space group $P2_1$ or $P2_1/m$, unit-cell parameters $a = 5.431(3)$, $b = 13.689(7)$, $c = 5.892(3)$ Å, $\beta = 111.79(4)°$, $Z = 2$. Since then, no further study has been reported for this mineral. Here, we present the first structure solution of bartelkeite from single-crystal X-ray-diffraction data, demonstrating that its ideal chemical formula is $PbFeGe_3O_7(OH)_2 \cdot H_2O$, rather than $PbFeGe_3O_8$. Furthermore, we reveal that bartelkeite is isostructural with the high-pressure $P2_1/m$ phase of rock-forming lawsonite, $CaAl_2Si_2O_7(OH) \cdot H_2O$, which is only stable above 8.6 GPa, opening a new channel for investigating the complex phase transitions in lawsonite.

EXPERIMENTAL PROCEDURES

The bartelkeite specimen used for the study is from the type locality, Tsumeb, Namibia, and in the collection of the RRUFF Project (http://rruff.info/R070114). Its chemical composition was determined using a Cameca SX-100 electron microprobe at 25 kV and 40 nA with a beam size of 10 μm. The average of 18 analysis points gives (wt%) PbO = 34.1(2), FeO = 10.6(1), GeO_2 = 46.2(2), As_2O_5 = 2.8(3), SiO_2 = 0.10(1), ZnO = 0.08(2), P_2O_5 = 0.04(1), Cl = 0.20(6), SO_3 = 0.14(4), and total = 94.4(2). The chemical formula was calculated on the basis of 10 (O + Cl) atoms per formula unit, as determined from the structure refinement (see below), by adding 5.64 wt% H_2O to achieve charge balance, yielding $Pb_{0.97}(Fe^{2+}_{0.94}Zn_{0.01})_{\Sigma=0.95}Ge^{VI}_{1.00}(Ge_{1.81}As_{0.16}Si_{0.01}S_{0.01})^{IV}_{\Sigma=1.99}O_7[(OH)_{1.94}Cl_{0.04}]_{\Sigma=1.98} \cdot 1.02H_2O$, which can be simplified as $PbFeGe^{VI}Ge_2^{IV}O_7(OH)_2 \cdot H_2O$.

Single-crystal X-ray diffraction data of bartelkeite were collected from a nearly equi-dimensional crystal (~0.09 × 0.09 × 0.08 mm) on a Bruker X8 APEX2 CCD X-ray diffractometer equipped with graphite-monochromatized Mo*K*α radiation.

* E-mail: hyang@u.arizona.edu

0003-004X/12/0010–1812$05.00/DOI: http://dx.doi.org/10.2138/am.2012.4269

Reflections with $I > 2\sigma(I)$ were indexed based on a monoclinic unit cell (Table 1). To facilitate a direct comparison with the high-pressure $P2_1/m$ structure of lawsonite (Pawley and Allan 2001), we adopted in this study a unit-cell setting (setting II in Table 1) differing from the one (setting I in Table 1) given by Keller et al. (1981). The matrix for the transformation from setting I to II is (0 0 –1/0 1 0/1 0 1). No satellite or super-lattice reflections were observed. The intensity data were corrected for X-ray absorption using the Bruker program SADABS. The systematic absences of reflections suggest possible space group $P2_1$ or $P2_1/m$. The crystal structure was solved and refined using SHELX97 (Sheldrick 2008) based on the space group $P2_1/m$, because it yielded a better refinement in terms of bond lengths and angles, atomic displacement parameters, and R factors. The positions of all atoms were refined with anisotropic displacement parameters, except for H atoms, which were refined with a fixed isotropic displacement parameter (U_{iso} = 0.03). During the structure refinements, ideal chemistry was assumed, as the overall effects of the trace amounts of other elements (Zn, As, Si, S, and Cl) on the final refined structure are negligible. Final refined atomic coordinates and displacement parameters are listed in Table 2 and selected bond lengths and angles in Table 3. A CIF is available[1].

The Raman spectrum of bartelkeite was recorded on a randomly oriented crystal from 12 scans at 30 s and 200 mW power per scan on a Thermo-Almega microRaman system, using a solid-state laser with a wavelength of 532 nm and a thermoelectrically cooled CCD detector. The laser is partially polarized with 4 cm^{-1} resolution and a spot size of 1 μm.

[1] Deposit item AM-12-097, CIF. Deposit items are available two ways: For a paper copy contact the Business Office of the Mineralogical Society of America (see inside front cover of recent issue) for price information. For an electronic copy visit the MSA web site at http://www.minsocam.org, go to the *American Mineralogist* Contents, find the table of contents for the specific volume/issue wanted, and then click on the deposit link there.

Results and discussion

Crystal structure

Most strikingly, bartelkeite is isostructural with the high-pressure $P2_1/m$ phase of lawsonite (Pawley and Allan 2001). Its structure consists of single chains of edge-sharing FeO_6 and $Ge1O_6$ octahedra parallel to the c-axis, cross-linked by $Ge2_2O_7$ tetrahedral dimers. The Pb atoms and H_2O groups occupy large cavities within the framework (Fig. 1). In fact, bartelkeite is the first known mineral containing both 4- and 6-coordinated Ge atoms. Compared to the $Ge1O_6$ octahedron, the FeO_6 octahedron is markedly distorted, as measured by the octahedral angle variance (OAV) and quadratic elongation (OQE) (Robinson et al. 1971). The OAV and OQE indexes are 136.4 and 1.042, respectively, for the FeO_6 octahedron, but only 11.4 and 1.004 for the $Ge1O_6$ octahedron. The pronounced distortion of the FeO_6 octahedron stems primarily from its edge-sharing with the smaller, more strongly bonded $Ge1O_6$ octahedron. To maintain such a linkage, the shared edges of the comparatively large and soft FeO_6 octahedron have to be shortened substantially to match those of the rigid GeO_6 octahedron, making the O-Fe-O angle subtending the shared edge (70.96°) deviate considerably from the ideal value of 90°. This is similar to the high-pressure $P2/n$ $Na(Mg_{0.5}Si_{0.5})Si_2O_6$ clinopyroxene, where MgO_6 and SiO_6 octahedra also share

Table 1. Summary of crystal data and refinement results for bartelkeite

	Bartelkeite (this study)		Bartelkeite (Keller et al. 1981)
	(setting I)	(setting II)	
Ideal chemical formula	$PbFeGe_3O_7(OH)2{\cdot}H_2O$		$PbFeGe_3O_8$
Space group	$P2_1/m$		$P2_1$ or $P2_1/m$
a (Å)	5.4033(2)	5.8279(2)	5.431(3)
b (Å)	13.6150(4)	13.6150(4)	13.689(7)
c (Å)	5.8279(2)	6.3097(2)	5.892(3)
β (°)	111.760(2)	127.314(2)	111.79(4)
V (Å^3)	398.19(3)	398.19(3)	406.7
Z	2		2
ρ_{calc} (g/cm^3)	5.36		4.97
λ (Å)	0.71073		
μ (mm^{-1})	34.08		
2θ range for data collection	≤70.11		
No. of reflections collected	8266		
No. of independent reflections	1798		
No. of reflections with $I > 2\sigma(I)$	1594		
No. of parameters refined	85		
R_{int}	0.029		
Final $R1$, $wR2$ factors [$I > 2\sigma(I)$]	0.023, 0.043		
Final $R1$, $wR2$ factors (all data)	0.028, 0.045		
Goodness-of-fit	1.024		

Note: The matrix for the transformation from setting I to II is (0 0 –1/0 1 0/ 1 0 1).

Table 3. Selected bond distances and angles in bartelkeite

	Distance (Å)		Distance (Å)
Pb-O1	2.703(3)	Fe-O3	2.043(2) x2
Pb-O2	2.645(2) x2	Fe-O4	2.213(2) x2
Pb-O3	2.473(2) x2	Fe-O5H	2.133(2) x2
Pb-O4	3.152(4) x2		
Pb-O6w	2.622(4)	Avg.	2.130
Pb-O6w	3.237(4)	OQE	1.042
		OAV	136.4
Avg.	2.789		
Ge1-O2	1.915(2) x2	Ge2-O1	1.754(1)
Ge1-O4	1.902(2) x2	Ge2-O2	1.734(2)
Ge1-O5H	1.849(2) x2	Ge2-O3	1.729(2)
		Ge2-O4	1.757(2)
Avg.	1.889	Avg.	1.744
OQE	1.004	TQE	1.007
OAV	11.4	TAV	26.8
O5H-H1	0.77(4)	O6w-H2	0.81(4)
O3···H1	2.02(4)	O5H···H2	2.03(4)
O5H···O3	2.761(3)	O6w···O5H	2.777(3)
∠O5H-H1-O3	160(5)°	∠O6w-H2-O5H	152(5)°

Table 2. Coordinates and displacement parameters of atoms in bartelkeite

Atom	x	y	z	U_{eq}	U_{11}	U_{22}	U_{33}	U_{23}	U_{13}	U_{12}
Pb	0.32486(4)	0.75	0.67674(3)	0.0149(1)	0.0142(1)	0.0155(1)	0.01618(8)	0	0.00984(7)	0
Fe	0.5	0	0	0.0077(1)	0.0082(3)	0.0087(3)	0.0066(2)	–0.0011(2)	0.0047(2)	–0.0016(2)
Ge1	0.5	0	0.5	0.0077(1)	0.0076(2)	0.0100(3)	0.0055(2)	0.0018(1)	0.0040(2)	0.0028(1)
Ge2	0.96137(6)	0.12998(3)	0.99604(6)	0.0069(1)	0.0058(1)	0.0072(2)	0.0065(1)	0.0001(1)	0.0032(1)	0.0005(1)
O1	0.9013(7)	0.75	0.9350(7)	0.0157(7)	0.011(1)	0.006(2)	0.027(2)	0	0.009(1)	0
O2	0.7512(5)	0.1115(2)	0.6545(4)	0.0128(5)	0.012(1)	0.015(1)	0.0084(9)	–0.0001(8)	0.0044(8)	–0.0031(8)
O3	0.7820(5)	0.3853(2)	0.1337(4)	0.0114(4)	0.013(1)	0.012(1)	0.0132(9)	0.0041(8)	0.0097(8)	0.0040(8)
O4	0.2838(4)	0.0625(2)	0.1610(4)	0.0088(4)	0.0083(9)	0.012(1)	0.0063(8)	0.0032(8)	0.0044(7)	0.0053(7)
O5H	0.2893(5)	0.0525(2)	0.6036(4)	0.0116(5)	0.0087(9)	0.018(1)	0.0074(8)	0.0017(8)	0.0046(7)	0.0037(8)
O6W	0.7617(9)	0.75	0.3216(8)	0.0240(8)	0.028(2)	0.012(2)	0.033(2)	0	0.019(2)	0
H1	0.143(6)	0.078(4)	0.495(7)	0.03*						
H2	0.713(8)	0.798(2)	0.355(9)	0.03*						

* U_{iso} fixed during refinement.

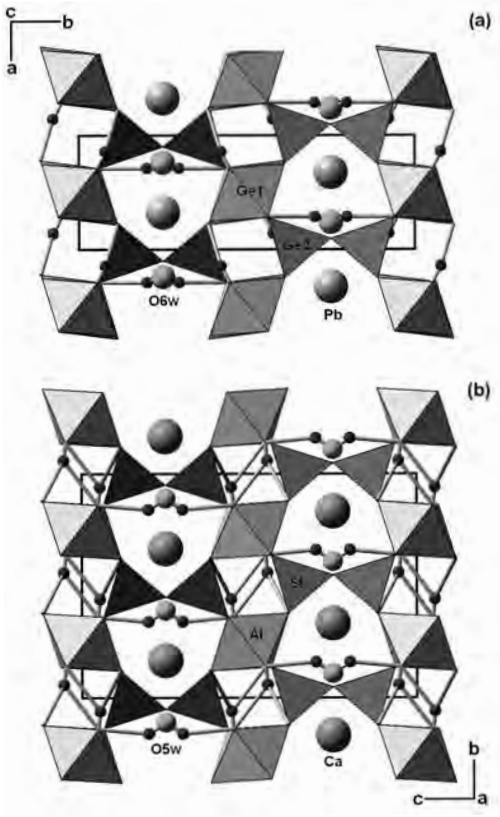

FIGURE 1. Comparison of crystal structures of (**a**) bartelkeite and (**b**) lawsonite at 295 K (Libowitzky and Armbruster 1995). The FeO_6 octahedra in bartelkeite are beneath the $Ge1O_6$ octahedra. The large, medium, and small spheres represent Pb, O6w, and H atoms, respectively, in bartelkeite, and Ca, O5w, and H atoms in lawsonite.

edges to form single chains (Angel et al. 1988; Yang et al. 2009) and the O-Mg-O angle subtending the shared edge is 69.5°.

The Pb^{2+} cation in bartelkeite, due probably to its lone-pair electron activities, displays a (6+3) coordination, with six Pb-O bond lengths shorter than 2.70 Å and three longer than 3.15 Å (Table 3). By comparison, Sr^{2+} in the isostructural $P2_1/m$ itoigawaite, $SrAl_2Si_2O_7(OH)_2 \cdot H_2O$, is also 9-coordinated, but with all Sr-O bond distances falling between 2.53 and 2.93 Å (Liebscher et al. 2010), despite its similar size to Pb^{2+} ($R_{Pb^{2+}}$ = 1.29 Å and $R_{Sr^{2+}}$ = 1.31 Å) (Shannon 1976). Likewise, Pb^{2+} in synthetic *Pbnm* Pb-lawsonite, $PbAl_2Si_2O_7(OH)_2 \cdot H_2O$, can also be considered 9-coordinated, with the Pb-O bond distances ranging from 2.48 to 3.11 Å (Dörsam et al. 2011).

Contrary to the work by Keller et al. (1981), our structure analysis clearly indicates the presence of both OH and H_2O in bartelkeite, as shown by our bond-valence calculations using the parameters given by Brese and O'Keeffe (1991) (Table 4), as well as by our Raman spectroscopic measurements (see below). The hydrogen bonding scheme in bartelkeite (Table 3) is similar to that in lawsonite. However, OH in bartelkeite appears to be engaged in only one hydrogen bond, but two in lawsonite (Fig. 1).

Raman spectra

The Raman spectrum of bartelkeite is plotted in Figure 2. Based on previous Raman spectroscopic studies on various germanate materials (e.g., Ross et al. 1986; Baran et al. 2004; Takahashi et al. 2008), we made the following tentative assignments for the major bands. The two broad bands at 3293 and 3490 cm^{-1} are due to O-H stretching vibrations. According to Libowitsky (1999), these two bands correspond to estimated O···O distances of ~2.75 and 2.95 Å, respectively, which are compared to the O5H···O3 (2.76 Å) and O6w···O5H (2.78 Å) distances from the structure refinement (Table 3). The very weak and broad band at 1558 cm^{-1} is characteristic of the H-O-H bending vibration. The two bands at 758 (the strongest) and 812 cm^{-1} are attributed to the symmetric and antisymmetric stretching vibrations of Ge-O bonds within the GeO_4 tetrahedron, respectively, whereas the band at 492 cm^{-1} is assigned to the Ge-O stretching vibrations within the GeO_6 octahedron. The two bands at 549 (the second strongest) and 393 cm^{-1} are ascribed to the Ge^{IV}-O-Ge^{IV} and Ge^{VI}-O-Ge^{IV} bending vibrations, respectively. The bands below 320 cm^{-1} are of complex nature and mostly associated with the rotational and translational modes of GeO_4 and GeO_6 polyhedra, Fe-O interactions, and the lattice vibrational modes.

TABLE 4. Bond-valence sums for bartelkeite

	Pb	Fe	Ge1	Ge2	∑O
O1	0.20	—	—	$^{2\rightarrow\times}$ 0.98	**2.16**
O2	$^{2\downarrow\times}$ 0.24	—	$^{2\downarrow\times}$ 0.63	1.04	**1.91**
O3	$^{2\downarrow\times}$ 0.38	$^{2\downarrow\times}$ 0.43	—	1.05	**1.86**
O4	$^{2\downarrow\times}$ 0.06	$^{2\downarrow\times}$ 0.27	$^{2\downarrow\times}$ 0.66	0.97	**1.96**
O5H	—	$^{2\downarrow\times}$ 0.34	$^{2\downarrow\times}$ 0.76	—	**1.10**
O6W	0.25				
	0.05	—	—	—	**0.30**
∑M	**1.86**	**2.08**	**4.10**	**4.04**	

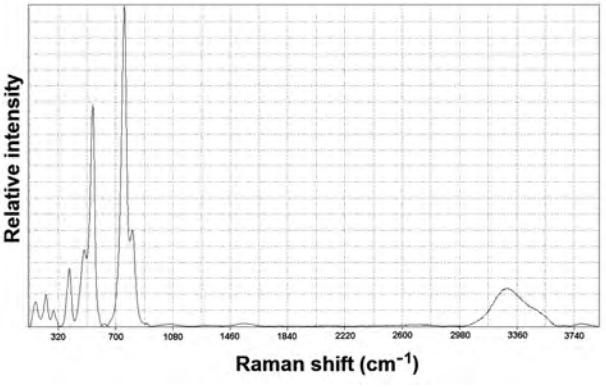

FIGURE 2. Raman spectrum of bartelkeite.

Implications for lawsonite

Lawsonite is an index mineral for high-pressure low-temperature metamorphism (such as blueschist facies). Its high-H_2O content (11.5 wt%) and high-pressure stability, up to ~12 GPa at 1240 K, make it a potential host for water in subducting slabs down to as much as 250 km (Pawley 1994; Schmidt 1995). Recent experimental studies have uncovered the intricate behavior of this mineral as a function of temperature, pressure, and composition. On the one hand, lawsonite undergoes two reversible phase transitions attributed to the order-disorder of hydrogen bonding at low temperatures, one from *Cmcm* to *Pmcn* at 273 K and the other from *Pmcn* to $P2_1cn$ at 155 K (Libowitzky and Armbruster

1995; Meyer et al. 2001; Sondergeld et al. 2005; Kolesov et al. 2008 and references therein). On the other hand, it exhibits an unquenchable, displacive transition from *Cmcm* to $P2_1/m$ at high pressures above 8.6 GPa (Daniel et al. 2000; Pawley and Allan 2001; Boffa Ballaran and Angel 2003). However, the stability field of this high-pressure $P2_1/m$ phase is still undefined. In addition, Liebscher et al. (2010) noticed a *Cmcm*-to-$P2_1/m$ symmetry change as the substitution of Sr for Ca increases in lawsonite, whereas Dörsam et al. (2011) synthesized *Pbnm* Pb-lawsonite, $PbAl_2Si_2O_7(OH)_2 \cdot H_2O$ at 2 GPa and 600 °C. The determination of the bartelkeite structure implies that the lawsonite- or bartelkeite-type structure or topologically similar structures can be rather compliant and complex, and a variety of such compounds with different cation sizes and valences may be synthesized or found in nature, such as $CaMgSi^{VI}(Si_2O_7)(OH)_2 \cdot H_2O$, $NaAlSi^{VI}(SiO_7)(OH)_2 \cdot H_2O$, $CaAlCr(Si_2O_7)(OH)_2 \cdot H_2O$, and $BaFeTi(Si_2O_7)(OH)_2 \cdot H_2O$. Furthermore, it suggests that bartelkeite-type compounds can serve as good models for further exploration of the temperature-pressure-composition space of lawsonite and the discovery of more exotic phases at various temperatures and pressures.

Acknowledgments

This study was funded by the Science Foundation Arizona.

References cited

Angel, R.J., Gasparik, T., Ross, N.L., Finger, L.W., Prewitt, C.T., and Hazen, R.M. (1988) A silica-rich sodium pyroxene phase with six-coordinated silicon. Nature, 335, 156–158.

Baran, E.J., Mercader, R.C., and Cascales, C. (2004) Vibrational and ^{57}Fe-Mössbauer spectra of $LaFeGe_2O_7$ and $NdFeGe_2O_7$. Journal of Physics and Chemistry of Solids, 65, 1913–1915.

Boffa Ballaran, T. and Angel, R.J. (2003) Equation of state and high-pressure phase transitions in lawsonite. European Journal of Mineralogy, 15, 241–246.

Brese, N.E. and O'Keeffe, M. (1991) Bond-valence parameters for solids. Acta Crystallographica, B47, 192–197.

Daniel, I., Fiquet, G., Gillet, P., Schmidt, M.W., and Hanfland, M. (2000) High-pressure behavior of lawsonite: a phase transition at 8.6 GPa. European Journal of Mineralogy, 21, 721–733.

Dörsam, G., Liebscher, A., Wunder, B., Franz, G., and Gottschalk, M. (2011) Synthesis of Pb-zoisite and Pb-lawsonite. Neues Jahrbuch für Mineralogie, Abhandlungen, 188, 99–110.

Frost, D.J. (2006) The stability of hydrous mantle phases. In H. Keppler and J.R. Smyth, Eds., Water in Nominally Anhydrous Minerals, 62, p. 243–271. Reviews in Mineralogy and Geochemistry, Mineralogical Society of America, Chantilly, Virginia.

Hazen, R.M., Downs, R.T., and Finger, L.W. (1996) High-pressure framework silicates. Science, 272, 1769–1771.

Henderson, G.S. and Wang, H.M. (2002) Germanium coordination and the germanate anomaly. European Journal of Mineralogy, 14, 733–744.

Iezzi, G., Boffa Ballaran, T., McCammon, C., and Langenhorst, F. (2005) The $CaGeO_3$–$Ca_3Fe_2Ge_3O_{12}$ garnet join: an experimental study. Physics and Chemistry of Minerals, 32, 197–207.

Keller, P., Hess, H., and Dunn, P., and Bartelkeit, J. (1981) $PbFe^{2+}Ge_3O_8$, ein neues Germanium-Mineral von Tsumeb, Namibia. Chemie der Erde, 40, 201–206.

Kolesov, B.A., Lager, G.A., and Schultz, A.J. (2008) Behaviour of H_2O and OH in lawsonite: a single-crystal neutron diffraction study and Raman spectroscopic investigation. European Journal of Mineralogy, 20, 63–72.

Libowitsky, E. (1999) Correlation of O–H stretching frequencies and O–H.O hydrogen bond lengths in minerals. Monatshefte für Chemie, 130, 1047–1059.

Libowitzky, E. and Armbruster, T. (1995) Low-temperature phase transitions and the role of hydrogen bonds in lawsonite. American Mineralogist, 80, 1277–1285.

Liebscher, A., Dörsam, G., Franz, G., Wunder, B., and Gottschalk, M. (2010) Crystal chemistry of synthetic lawsonite solid-solution series $CaAl_2[(OH)_2/Si_2O_7] \cdot H_2O$-$SrAl_2[(OH)_2/Si_2O_7] \cdot H_2O$ and the *Cmcm*-$P2_1/m$ phase transition. American Mineralogist, 95, 724–735.

Meyer, H-W., Marion, S., Carpenter, M.A., Knight, K.S., Redfern, S.A.T., and Dove, M.T. (2001) Displacive components of the low temperature phase transitions in lawsonite. American Mineralogist, 86, 566–577.

Nestola, F., Németh, P., Angel, R.J., and Buseck, P.R. (2008) Equation of state and crystal structure of a new germanate post-titanite phase. American Mineralogist, 93, 1424–1428.

Pawley, A.R. (1994) The pressure and temperature stability limits of lawsonite: Implications for H_2O recycling in subduction zones. Contributions to Mineralogy and Petrology, 118, 99–108.

Pawley, A.R. and Allan, D.R. (2001) A high-pressure structural study of lawsonite using angle-dispersive powder-diffraction methods with synchrotron radiation. Mineralogical Magazine, 65, 41–58.

Ringwood, A.E. and Major, A. (1967) High-pressure reconnaissance investigations in the system Mg_2SiO_4-MgO-H_2O. Earth and Planetary Science Letters, 2, 130–133.

Ringwood, A.E. and Seabrook, M. (1963) High-pressure phase transitions in germanate pyroxenes and related compounds. Journal of Geophysical Research, 68, 4601–4609.

Robinson, K., Gibbs, G.V., and Ribbe, P.H. (1971) Quadratic elongation: a quantitative measure of distortion in coordination polyhedra. Science, 172, 567–570.

Ross, N.L., Akaogi, M., Navrotsky, A., Susaki, J.I., and McMillan, P. (1986) Phase transitions among the $CaGeO_3$ polymorphs (wollastonite, garnet and perovskite structures): studies by high-pressure synthesis, high-temperature calorimetry, and vibrational spectroscopy and calculation. Journal of Geophysical Research, 91, 4685–4696.

Schmidt, M.W. (1995) Lawsonite: upper pressure stability and formation of higher density hydrous phases. American Mineralogist, 80, 1286–1292.

Shannon, R.D. (1976) Revised effective ionic radii and systematic studies of interatomic distances in halides and chalcogenides. Acta Crystallographica, A32, 751–767.

Sheldrick, G.M. (2008) A short history of *SHELX*. Acta Crystallographica, A64, 112–122.

Sondergeld, P., Schranz, W., Tröster, A., Armbruster, T., Giester, G., Kityk, A., and Carpenter, M.A. (2005) Ordering and elasticity associated with low-temperature phase transitions in lawsonite. American Mineralogist, 90, 448–456.

Takahashi, Y., Iwashaki, K., Masai, H., and Fujiwara, T. (2008) Raman spectroscopic study of benitoite-type compounds. Journal of the Ceramics Society of Japan, 116, 1139–1142.

Thomas, S-M., Müller, M.K., Kahlenberg, V., Thomas, B., Rhede, D., Wirth, R., and Wunder, B. (2008) Protonation in germanium equivalents of ringwoodite, anhydrous phase B, and superhydrous phase B. American Mineralogist, 93, 1282–1294.

Thompson, A.B. (1992) Water in the Earth's upper mantle. Nature, 358, 295–302.

Wunder, B. and Marler, B. (1997) Ge-analogues of aluminium silicates: High-pressure synthesis and properties of orthorhombic $Al_2GeO_4(OH)_2$. European Journal of Mineralogy, 9, 1147–1158.

Yang, H., Konzett, J., Frost, D.J., and Downs, R.T. (2009) X-ray diffraction and Raman spectroscopic studies of clinopyroxenes with six-coordinated Si in the $Na(Mg_{0.5}Si_{0.5})Si_2O_6$-$NaAlSi_2O_6$ system. American Mineralogist, 94, 942–949.

Manuscript received June 19, 2012
Manuscript accepted July 15, 2012
Manuscript handled by Ian Swainson

```
data_bart2

_audit_creation_method            SHELXL-97
_chemical_name_systematic
;
 ?
;
_chemical_name_common             ?
_chemical_melting_point           ?
_chemical_formula_moiety          ?
_chemical_formula_sum
 'H2 Fe Ge3 O10 Pb'
_chemical_formula_weight          642.83

loop_
 _atom_type_symbol
 _atom_type_description
 _atom_type_scat_dispersion_real
 _atom_type_scat_dispersion_imag
 _atom_type_scat_source
 'O'  'O'   0.0106   0.0060
 'International Tables Vol C Tables 4.2.6.8 and 6.1.1.4'
 'H'  'H'   0.0000   0.0000
 'International Tables Vol C Tables 4.2.6.8 and 6.1.1.4'
 'Fe'  'Fe'   0.3463   0.8444
 'International Tables Vol C Tables 4.2.6.8 and 6.1.1.4'
 'Ge'  'Ge'   0.1547   1.8001
 'International Tables Vol C Tables 4.2.6.8 and 6.1.1.4'
 'Pb'  'Pb'  -3.3944  10.1111
 'International Tables Vol C Tables 4.2.6.8 and 6.1.1.4'

_symmetry_cell_setting            ?
_symmetry_space_group_name_H-M    ?

loop_
 _symmetry_equiv_pos_as_xyz
 'x, y, z'
 '-x, y+1/2, -z'
 '-x, -y, -z'
 'x, -y-1/2, z'

_cell_length_a                    5.8279(2)
_cell_length_b                    13.6150(4)
_cell_length_c                    6.3097(2)
_cell_angle_alpha                 90.00
_cell_angle_beta                  127.314(2)
_cell_angle_gamma                 90.00
_cell_volume                      398.18(2)
_cell_formula_units_Z             2
_cell_measurement_temperature     293(2)
_cell_measurement_reflns_used     ?
_cell_measurement_theta_min       ?
_cell_measurement_theta_max       ?

_exptl_crystal_description        ?
```

```
_exptl_crystal_colour             ?
_exptl_crystal_size_max           ?
_exptl_crystal_size_mid           ?
_exptl_crystal_size_min           ?
_exptl_crystal_density_meas       ?
_exptl_crystal_density_diffrn     5.362
_exptl_crystal_density_method     'not measured'
_exptl_crystal_F_000              572
_exptl_absorpt_coefficient_mu     34.083
_exptl_absorpt_correction_type    ?
_exptl_absorpt_correction_T_min   ?
_exptl_absorpt_correction_T_max   ?
_exptl_absorpt_process_details    ?

_exptl_special_details
;
 ?
;

_diffrn_ambient_temperature       293(2)
_diffrn_radiation_wavelength      0.71073
_diffrn_radiation_type            MoK\a
_diffrn_radiation_source          'fine-focus sealed tube'
_diffrn_radiation_monochromator   graphite
_diffrn_measurement_device_type   ?
_diffrn_measurement_method        ?
_diffrn_detector_area_resol_mean  ?
_diffrn_standards_number          ?
_diffrn_standards_interval_count  ?
_diffrn_standards_interval_time   ?
_diffrn_standards_decay_%         ?
_diffrn_reflns_number             8260
_diffrn_reflns_av_R_equivalents   0.0340
_diffrn_reflns_av_sigmaI/netI     0.0328
_diffrn_reflns_limit_h_min        -9
_diffrn_reflns_limit_h_max        9
_diffrn_reflns_limit_k_min        -19
_diffrn_reflns_limit_k_max        21
_diffrn_reflns_limit_l_min        -10
_diffrn_reflns_limit_l_max        10
_diffrn_reflns_theta_min          2.99
_diffrn_reflns_theta_max          35.05
_reflns_number_total              1797
_reflns_number_gt                 1593
_reflns_threshold_expression      >2sigma(I)

_computing_data_collection        ?
_computing_cell_refinement        ?
_computing_data_reduction         ?
_computing_structure_solution     'SHELXS-97 (Sheldrick, 1990)'
_computing_structure_refinement   'SHELXL-97 (Sheldrick, 1997)'
_computing_molecular_graphics     ?
_computing_publication_material   ?

_refine_special_details
;
 Refinement of F^2^ against ALL reflections.  The weighted R-factor wR and
```

```
 goodness of fit S are based on F^2^, conventional R-factors R are based
 on F, with F set to zero for negative F^2^. The threshold expression of
 F^2^ > 2sigma(F^2^) is used only for calculating R-factors(gt) etc. and is
 not relevant to the choice of reflections for refinement.  R-factors based
 on F^2^ are statistically about twice as large as those based on F, and R-
 factors based on ALL data will be even larger.
;

_refine_ls_structure_factor_coef  Fsqd
_refine_ls_matrix_type            full
_refine_ls_weighting_scheme       calc
_refine_ls_weighting_details
 'calc w=1/[\s^2^(Fo^2^)+(0.0178P)^2^+0.0000P] where P=(Fo^2^+2Fc^2^)/3'
_atom_sites_solution_primary      direct
_atom_sites_solution_secondary    difmap
_atom_sites_solution_hydrogens    geom
_refine_ls_hydrogen_treatment     mixed
_refine_ls_extinction_method      SHELXL
_refine_ls_extinction_coef        0.0024(2)
_refine_ls_extinction_expression
 'Fc^*^=kFc[1+0.001xFc^2^\l^3^/sin(2\q)]^-1/4^'
_refine_ls_number_reflns          1797
_refine_ls_number_parameters      83
_refine_ls_number_restraints      2
_refine_ls_R_factor_all           0.0283
_refine_ls_R_factor_gt            0.0230
_refine_ls_wR_factor_ref          0.0441
_refine_ls_wR_factor_gt           0.0430
_refine_ls_goodness_of_fit_ref    1.029
_refine_ls_restrained_S_all       1.031
_refine_ls_shift/su_max           0.004
_refine_ls_shift/su_mean          0.000

loop_
 _atom_site_label
 _atom_site_type_symbol
 _atom_site_fract_x
 _atom_site_fract_y
 _atom_site_fract_z
 _atom_site_U_iso_or_equiv
 _atom_site_adp_type
 _atom_site_occupancy
 _atom_site_symetry_multiplicity
 _atom_site_calc_flag
 _atom_site_refinement_flags
 _atom_site_disorder_assembly
 _atom_site_disorder_group
Pb Pb 0.32487(4) 0.7500 0.67674(3) 0.01488(6) Uani 1 2 d S . .
Fe Fe 0.5000 0.0000 0.0000 0.00769(12) Uani 1 2 d S . .
Ge1 Ge 0.5000 0.0000 0.5000 0.00773(9) Uani 1 2 d S . .
Ge2 Ge 0.96137(6) 0.12998(3) 0.99604(6) 0.00688(7) Uani 1 1 d . . .
O1 O 0.9013(7) 0.7500 0.9350(7) 0.0157(7) Uani 1 2 d S . .
O2 O 0.7512(5) 0.11151(19) 0.6545(4) 0.0128(5) Uani 1 1 d . . .
O3 O 0.7821(5) 0.38529(19) 0.1337(4) 0.0114(4) Uani 1 1 d . . .
O4 O 0.2837(4) 0.06250(19) 0.1610(4) 0.0088(4) Uani 1 1 d . . .
O5H O 0.2893(5) 0.0524(2) 0.6036(4) 0.0116(5) Uani 1 1 d D . .
O6W O 0.7617(9) 0.7500 0.3216(8) 0.0239(8) Uani 1 2 d SD . .
```

```
H1 H 0.144(8) 0.077(4) 0.497(8) 0.030 Uiso 1 1 d D . .
H2 H 0.712(9) 0.799(3) 0.356(9) 0.030 Uiso 1 1 d D . .

loop_
 _atom_site_aniso_label
 _atom_site_aniso_U_11
 _atom_site_aniso_U_22
 _atom_site_aniso_U_33
 _atom_site_aniso_U_23
 _atom_site_aniso_U_13
 _atom_site_aniso_U_12
Pb 0.01415(8) 0.01555(11) 0.01618(8) 0.000 0.00984(7) 0.000
Fe 0.0082(3) 0.0087(4) 0.0066(2) -0.00110(19) 0.0047(2) -0.0016(2)
Ge1 0.00759(18) 0.0100(3) 0.00554(16) 0.00176(14) 0.00397(15) 0.00282(14)
Ge2 0.00581(13) 0.00720(18) 0.00654(12) 0.00011(10) 0.00318(10) 0.00054(10)
O1 0.0105(14) 0.0064(19) 0.0266(17) 0.000 0.0093(13) 0.000
O2 0.0120(10) 0.0146(14) 0.0084(8) -0.0001(8) 0.0044(8) -0.0031(8)
O3 0.0129(10) 0.0117(13) 0.0132(9) 0.0042(8) 0.0097(8) 0.0040(8)
O4 0.0083(9) 0.0119(12) 0.0063(8) 0.0032(8) 0.0044(7) 0.0053(7)
O5H 0.0087(9) 0.0179(15) 0.0074(8) 0.0017(8) 0.0046(8) 0.0037(8)
O6W 0.028(2) 0.012(2) 0.033(2) 0.000 0.0190(17) 0.000

_geom_special_details
;
 All esds (except the esd in the dihedral angle between two l.s. planes)
 are estimated using the full covariance matrix.  The cell esds are taken
 into account individually in the estimation of esds in distances, angles
 and torsion angles; correlations between esds in cell parameters are only
 used when they are defined by crystal symmetry.  An approximate (isotropic)
 treatment of cell esds is used for estimating esds involving l.s. planes.
;

loop_
 _geom_bond_atom_site_label_1
 _geom_bond_atom_site_label_2
 _geom_bond_distance
 _geom_bond_site_symmetry_2
 _geom_bond_publ_flag
Pb O3 2.473(2) 2_656 ?
Pb O3 2.473(2) 3_666 ?
Pb O6W 2.623(4) 1_455 ?
Pb O2 2.645(2) 2_656 ?
Pb O2 2.645(2) 3_666 ?
Pb O1 2.703(3) . ?
Fe O3 2.042(2) 4_565 ?
Fe O3 2.042(2) 2_645 ?
Fe O5H 2.133(2) 1_554 ?
Fe O5H 2.133(2) 3_656 ?
Fe O4 2.213(2) 3_655 ?
Fe O4 2.213(2) . ?
Ge1 O5H 1.849(2) 3_656 ?
Ge1 O5H 1.849(2) . ?
Ge1 O4 1.902(2) 3_656 ?
Ge1 O4 1.902(2) . ?
Ge1 O2 1.915(2) . ?
Ge1 O2 1.915(2) 3_656 ?
Ge2 O3 1.729(2) 4_566 ?
```

```
Ge2 O2 1.734(2) . ?
Ge2 O1 1.7544(12) 3_767 ?
Ge2 O4 1.757(2) 1_656 ?
O1 Ge2 1.7544(12) 3_767 ?
O1 Ge2 1.7544(12) 2_757 ?
O2 Pb 2.645(2) 3_666 ?
O3 Ge2 1.729(2) 4_564 ?
O3 Fe 2.042(2) 2_655 ?
O3 Pb 2.473(2) 3_666 ?
O4 Ge2 1.757(2) 1_454 ?
O5H Fe 2.133(2) 1_556 ?
O5H H1 0.77(4) . ?
O6W Pb 2.623(4) 1_655 ?
O6W H2 0.81(4) . ?

loop_
 _geom_angle_atom_site_label_1
 _geom_angle_atom_site_label_2
 _geom_angle_atom_site_label_3
 _geom_angle
 _geom_angle_site_symmetry_1
 _geom_angle_site_symmetry_3
 _geom_angle_publ_flag
O3 Pb O3 96.29(11) 2_656 3_666 ?
O3 Pb O6W 82.03(8) 2_656 1_455 ?
O3 Pb O6W 82.03(8) 3_666 1_455 ?
O3 Pb O2 160.47(7) 2_656 2_656 ?
O3 Pb O2 83.14(8) 3_666 2_656 ?
O6W Pb O2 78.55(8) 1_455 2_656 ?
O3 Pb O2 83.14(8) 2_656 3_666 ?
O3 Pb O2 160.47(7) 3_666 3_666 ?
O6W Pb O2 78.55(8) 1_455 3_666 ?
O2 Pb O2 90.93(11) 2_656 3_666 ?
O3 Pb O1 107.09(7) 2_656 . ?
O3 Pb O1 107.09(7) 3_666 . ?
O6W Pb O1 165.86(12) 1_455 . ?
O2 Pb O1 91.61(7) 2_656 . ?
O2 Pb O1 91.61(7) 3_666 . ?
O3 Fe O3 180.00(9) 4_565 2_645 ?
O3 Fe O5H 88.59(9) 4_565 1_554 ?
O3 Fe O5H 91.41(9) 2_645 1_554 ?
O3 Fe O5H 91.41(9) 4_565 3_656 ?
O3 Fe O5H 88.59(9) 2_645 3_656 ?
O5H Fe O5H 180.00(14) 1_554 3_656 ?
O3 Fe O4 86.79(9) 4_565 3_655 ?
O3 Fe O4 93.21(9) 2_645 3_655 ?
O5H Fe O4 70.95(8) 1_554 3_655 ?
O5H Fe O4 109.05(8) 3_656 3_655 ?
O3 Fe O4 93.21(9) 4_565 . ?
O3 Fe O4 86.79(9) 2_645 . ?
O5H Fe O4 109.05(8) 1_554 . ?
O5H Fe O4 70.95(8) 3_656 . ?
O4 Fe O4 180.00(13) 3_655 . ?
O5H Ge1 O5H 180.0 3_656 . ?
O5H Ge1 O4 95.48(9) 3_656 3_656 ?
O5H Ge1 O4 84.52(9) . 3_656 ?
O5H Ge1 O4 84.52(9) 3_656 . ?
```

```
O5H Ge1 O4 95.48(9) . . ?
O4 Ge1 O4 180.00(10) 3_656 . ?
O5H Ge1 O2 91.13(11) 3_656 . ?
O5H Ge1 O2 88.87(11) . . ?
O4 Ge1 O2 90.07(10) 3_656 . ?
O4 Ge1 O2 89.93(10) . . ?
O5H Ge1 O2 88.87(11) 3_656 3_656 ?
O5H Ge1 O2 91.13(11) . 3_656 ?
O4 Ge1 O2 89.93(10) 3_656 3_656 ?
O4 Ge1 O2 90.07(10) . 3_656 ?
O2 Ge1 O2 180.00(10) . 3_656 ?
O3 Ge2 O2 114.84(11) 4_566 . ?
O3 Ge2 O1 108.13(14) 4_566 3_767 ?
O2 Ge2 O1 108.40(14) . 3_767 ?
O3 Ge2 O4 113.22(10) 4_566 1_656 ?
O2 Ge2 O4 110.89(11) . 1_656 ?
O1 Ge2 O4 100.19(13) 3_767 1_656 ?
Ge2 O1 Ge2 137.32(19) 3_767 2_757 ?
Ge2 O1 Pb 111.28(10) 3_767 . ?
Ge2 O1 Pb 111.28(10) 2_757 . ?
Ge2 O2 Ge1 119.58(13) . . ?
Ge2 O2 Pb 122.17(12) . 3_666 ?
Ge1 O2 Pb 116.90(9) . 3_666 ?
Ge2 O3 Fe 117.68(12) 4_564 2_655 ?
Ge2 O3 Pb 124.03(13) 4_564 3_666 ?
Fe O3 Pb 113.18(9) 2_655 3_666 ?
Ge2 O4 Ge1 129.93(11) 1_454 . ?
Ge2 O4 Fe 129.13(10) 1_454 . ?
Ge1 O4 Fe 99.83(9) . . ?
Ge1 O5H Fe 104.58(10) . 1_556 ?
Ge1 O5H H1 118(4) . . ?
Fe O5H H1 136(4) 1_556 . ?
Pb O6W H2 104(3) 1_655 . ?

loop_
 _geom_hbond_atom_site_label_D
 _geom_hbond_atom_site_label_H
 _geom_hbond_atom_site_label_A
 _geom_hbond_distance_DH
 _geom_hbond_distance_HA
 _geom_hbond_distance_DA
 _geom_hbond_angle_DHA
 _geom_hbond_site_symmetry_A
O5H H1 O3  0.77(4) 2.02(4) 2.761(3) 160(5) 4_465
O6W H2 O5H  0.81(4) 2.03(4) 2.777(3) 152(5) 3_666

_diffrn_measured_fraction_theta_max    0.986
_diffrn_reflns_theta_full              35.05
_diffrn_measured_fraction_theta_full   0.986
_refine_diff_density_max    1.953
_refine_diff_density_min   -1.194
_refine_diff_density_rms    0.256
```